Revista Brasileira de Meteorologia, **v. 36, n. 1,** 63−77, 2021
DOI: http://dx.doi.org/10.1590/0102-77863540083

Article

Prediction of Atmospheric Turbulence Characteristics for Surface Boundary Layer Using Empirical Spectral Methods

Yagya Dutta Dwivedi[1], Vasishta Bhargava Nukala[2], Satya Prasad Maddula[3], Kiran Nair[4]

[1]*Department of Aeronautical Engineering, Institute of Aeronautical Engineering, Hyderabad, India.*
[2]*Department of Mechanical Engineering, Sreyas Institute of Engineering and Technology, Hyderabad, India.*
[3]*Department of Aerospace Engineering, GITAM University, Hyderabad, India.*
[4]*Wind Resources, Mytrah Energy India Private Limited, Hyderabad, India.*

Received: 20 January 2020 - Accepted: 29 September 2020

Abstract

Atmospheric turbulence is an unsteady phenomenon found in nature and plays significance role in predicting natural events and life prediction of structures. In this work, turbulence in surface boundary layer has been studied through empirical methods. Computer simulation of Von Karman, Kaimal methods were evaluated for different surface roughness and for low (1%), medium (10%) and high (50%) turbulence intensities. Instantaneous values of one minute time series for longitudinal turbulent wind at mean wind speed of 12 m/s using both spectra showed strong correlation in validation trends. Influence of integral length scales on turbulence kinetic energy production at different heights is illustrated. Time series for mean wind speed of 12 m/s with surface roughness value of 0.05 m have shown that variance for longitudinal, lateral and vertical velocity components were different and found to be anisotropic. Wind speed power spectral density from Davenport and Simiu profiles have also been calculated at surface roughness of 0.05 m and compared with k^{-1} and k^{-3} slopes for Kolmogorov $k^{-5/3}$ law in inertial sub-range and k^{-7} in viscous dissipation range. At high frequencies, logarithmic slope of Kolmogorov $-5/3^{rd}$ law agreed well with Davenport, Harris, Simiu and Solari spectra than at low frequencies.

Keywords: turbulence, wind speed, spectra, length scale, surface roughness.

Predição de Características de Turbulência Atmosférica Para Camada Limite de Superfície Usando Métodos Espectrais Empíricos

Resumo

A turbulência atmosférica é um fenômeno instável encontrado na natureza e desempenha um papel significativo na previsão de eventos naturais e na previsão da vida de estruturas. Neste trabalho, a turbulência na camada limite superficial foi estudada por meio de métodos empíricos. Simulação computacional de Von Karman, métodos Kaimal foram avaliados para diferentes rugosidades superficiais e para intensidades de turbulência baixa (1%), média (10%) e alta (50%). Valores instantâneos de séries temporais de um minuto para vento turbulento longitudinal com velocidade média do vento de 12 m/s usando ambos os espectros mostraram forte correlação nas tendências de validação. A influência das escalas de comprimento integral na produção de energia cinética de turbulência em diferentes alturas é ilustrada. Séries temporais para velocidade média do vento de 12 m / s com rugosidade de superfície de 0,05 m mostraram que a variância para os componentes de velocidade longitudinal, lateral e vertical foram diferentes e considerados anisotrópicos. A densidade espectral da potência da velocidade do vento dos perfis de Davenport e Simiu também foi calculada na rugosidade da superfície de 0,05 m e comparada com inclinações k^{-1} e k^{-3} para a lei Kolmogorov $k^{5/3}$ em subfaixa inercial e k^{-7} em viscoso faixa de dissipação. Em altas frequências, a inclinação logarítmica da lei Kolmogorov $-5/3^{rd}$ concordou bem com os espectros de Davenport, Harris, Simiu e Solari do que em baixas frequências.

Palavras-chave: turbulência, velocidade do vento, espectros, escala de comprimento, rugosidade da superfície.

Send correspondence to Vasishta Bhargava Nukala, vasishtab@gmail.com.

1. Introduction

Research in field of turbulence has important applications in several fields of engineering. Turbulence characterization was done by Prandtl and Reynolds (Frank, 2011) who investigated turbulence phenomenon in atmospheric flows using experiments. In general turbulence can be defined as random and fluctuating motion of wind speed about its mean value and attributed to shear forces or friction between the layers of atmosphere caused either due to velocity or temperature gradients in atmospheric boundary layer. The former is known as *mechanical or shear turbulence* and latter is called *convective or thermal turbulence* (Lungu and Van Gelder, 1997). Integral length scale and turbulence intensity are important parameters to describe the scale of turbulent eddies and energy content available in them. Empirical and statistical turbulence models proposed by Kolmogorov (1991), Von Karman (1948), Solari (1987), Simiu (1974), Harris (1971), Davenport (1961), Teunissen (1980), Olesen *et al*. (1984) are based on friction velocity in atmospheric boundary layer. The coefficients in these spectra represent the spectral frequency range and the exponents in numerator and denominator determines the spectral shape (Wieringa, 1992; Jing and Lee, 1998; Van der Hoven, 1957). On the other hand Von Karman type models are dependent on the mean value of fluctuating wind speed component and integral length scales that vary with altitude. In this category, Harris (1971) is regarded as Von Karman type spectrum. The Harris (1971), Simiu (1974) in functional form has been adopted by ESDU (Engineering Science and Data Unit) and NBS (National Bureau of Standards) that are suitable for weather prediction. Jing and Lee (1998) in his study has obtained measured wind speed data from weather bureau of Taiwan and found that the longitudinal velocity spectra suggested by Kaimal (1972) and Simiu (1974) is more realistic and closely match with actual wind speed. Further, they proposed custom spectra similar to Von Karman type and fitted the data in energy containing and inertial sub-range as well as dissipation range. Different countries have adopted specific wind codes in order to characterize wind turbulence in atmosphere. The Solari spectrum has been successfully used by American wind code (ANSI/ASCE 7-10) while Japanese (AIJ/RLB 2004) and Australian (AS/NZS 1170.2-2002) wind codes use Von Karman like spectrum. The Chinese and Canadian wind codes have adopted Davenport spectrum while the Euro norm recommends similar type of wind spectrum as that of American wind code and resembles Solari spectrum. The Panofsky and Dutton (1984), Dyrbye and Hansen (1997), and Mann (1994) uniform shear stress turbulence spectrum models also make use of length scales to describe the size of turbulent eddies from small to large scales. To analyze turbulent boundary layers in surface layer in atmosphere, it is important to estimate the turbulent fluxes which are dynamic and unsteady in nature. An experimental analysis for in-situ measured wind speed was performed by Soltys *et al.* (2012) using a GILL R3-100 anemometer positioned at ~ 20 m from above ground level (AGL). They found fluctuating component of wind can be quantified by statistical correlation for analyzing spatial-temporal properties in frequency domain by means of wind power spectra density functions relevant to stability of structures. Lien and Sanford (2004) verified the Monin-Obukhov (M-O) similarity scaling theory for the ocean bottom boundary layer using wave spectra. They found that for a stratified boundary layer, buoyancy fluxes are important parameters in M-O scaling theory, however their study provided evidence for local similarity scaling in ocean bottom boundary layer where the buoyancy flux is negligible and M-O similarity theory breaks down. In another study by Mahrt *et al.* (2015) the importance of turbulence quantities on wind speed fluctuations based on friction velocity and heat flux parameters in stratified nocturnal atmospheric boundary layer (Taylor, 1971). Particularly the dependence of turbulent velocities on transitions that occur between weak wind and strong wind regimes were identified based on the spectral slopes. Further, a correlation between turbulence and wind speed fluctuations was established based on the shallow pool experiment data measured for a flat surface above a valley.

Research by Clement and Moncrieff (2019) showed that use of statistics based functional covariance flux approach to analyze the vertical turbulent transport fluxes within surface boundary layers yielded coherent agreements for measured parameters. However, they found that temporal averaging for eddy covariance is suboptimal in nature since the turbulent flux estimation through such methods introduces high uncertainty in the measured data. Furthermore research conducted by Serafin *et al.* (2018) showed that use of Numerical Weather Prediction models (NWP) in exchange of heat, mass and momentum over mountainous terrains at synoptic scale dynamics and thermally driven meso scale circulations. They also demonstrated the surface energy balance on mountain sites and provided an understanding of implications of measure data processed on the estimates of turbulence statistics. Also Chougule *et al.* (2015; 2018) have demonstrated that single point measurements of wind speed up to height of 100 m considering vertical mean wind speed and temperature gradients based on M-O similarity theory for stable and unstable stratified boundary layers. Computational methods such as direct numerical simulation (DNS) typically resolve all scales of motion in turbulent flows but large eddy simulation (LES) resolves only large scale eddy motion, approximating the small scales of motion. Hence, accuracy is difficult to measure in both DNS and LES when predicting turbulent flows. So, use of empirical methods is recommended to predict the turbulent flows at relatively low computational time and cost.

This paper is organized as follows: Section 2 describes about atmospheric boundary layer classification and topographic characteristics. Section 3 focuses on the empirical spectral methods that are aimed at characterizing atmospheric turbulence within the surface boundary layer. Factors which affect the quality of turbulence models, viz. surface roughness, turbulence intensity and length scales are discussed. Section 4 discusses the results obtained for a given surface roughness computer simulation of longitudinal wind speed for one minute using isotropic Von Karman and Kaimal methods. Occurrence of wind gust has been demonstrated by means of different time scales to understand the loading aspect on structures relevant to wind turbine components up to a height of 150 m where anisotropic turbulence is dominant. Power spectra of wind speed components have also been illustrated for different turbulence intensities based on Kaimal and Von Karman type methods. Finally, Section 5 presents the conclusions and future work for possible improvement of empirical methods.

2. Atmospheric Boundary Layer Height Classification and Topographical Characteristics

From Fig. 1(a) the boundary layer height is classified according to the surface roughness in *m*. It can be seen that lowest boundary layer can be termed as canopy layer in which the small scale eddies are evident. However, the shear stress is constant with negligible Coriolis forces with varying surface roughness and temperature gradients (Sutton, 1953). The eddies are caused due to tall trees up to 30-45 m above the ground level in which there is high obstruction of sunlight. Second region extends from 500 m to 1 km and influenced by Coriolis forces, surface roughness and temperature fluxes (Kaimal and Finnigan, 1994). Forces within the atmospheric boundary layer can be classified in terms of macro scale motion for heights greater than 20 km. Meso scale motions range in heights between 1 km to 20 km while micro scale motions are typically observed below 1 km where the shear stresses are dominant and common in surface boundary layer. It can also be

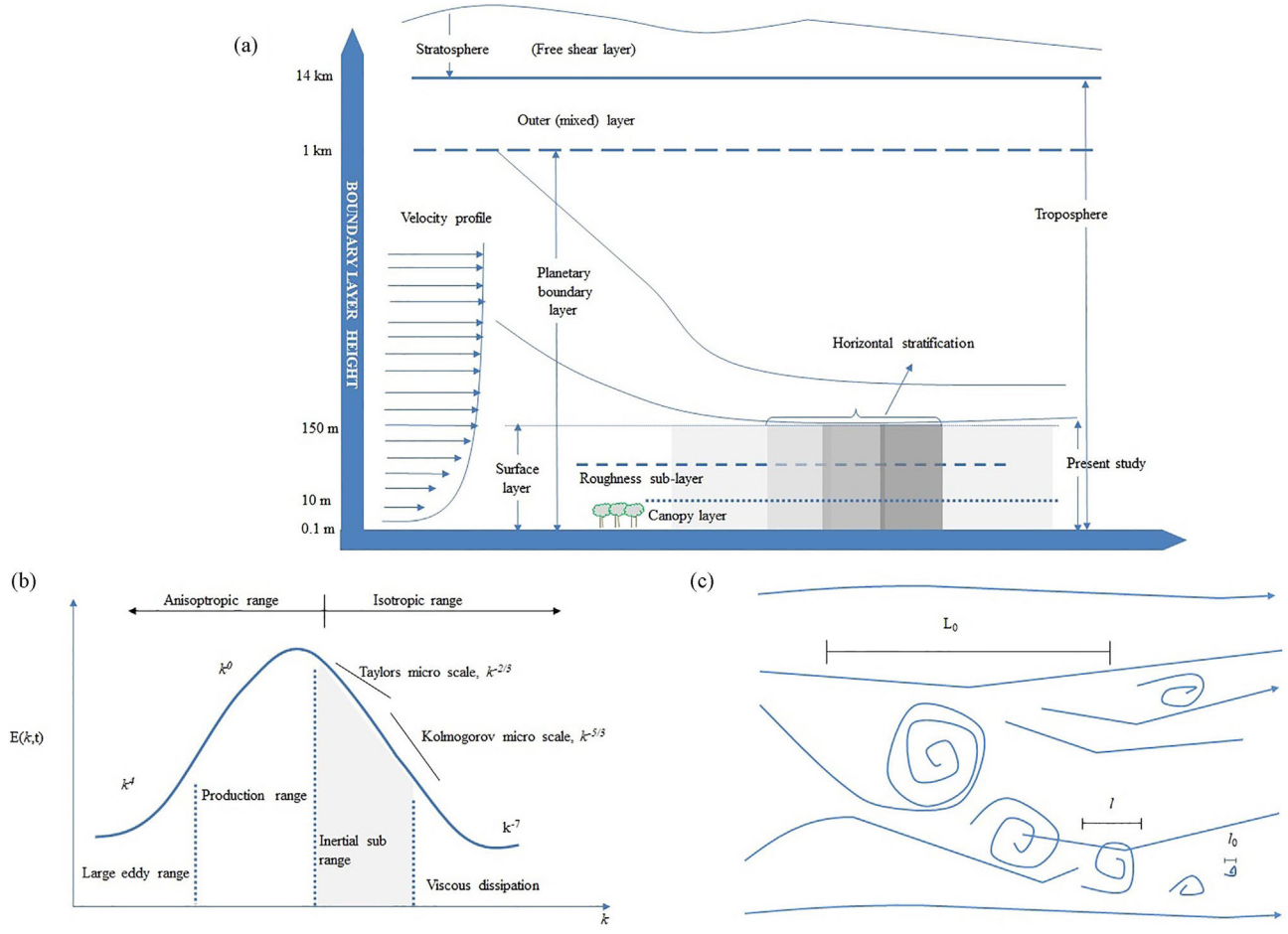

Figure 1 - (a) Illustration of boundary layer heights in terms of different roughness scales (b) Power spectra depicting turbulent kinetic energy in large eddy scales, production, inertial and viscous dissipation range (Mikkelsen *et al.*, 2017) (c) Atmospheric turbulence and its evolution showing the damping nature of eddy size by means of length scales (Adapted from (Chaudhary and Abhilash, 2012)).

seen that velocity profile within the surface layer is influenced by frictional shear force per unit area of the terrain and affects the momentum transport or momentum flux within the boundary layer. The surface boundary layer extends beyond the canopy layer and the roughness sublayer from where the eddies grow to large scale. The turbulent nature of eddies is isotropic if kinetic energy does not vary in longitudinal, lateral and vertical directions, however, for eddy surface layer the energy content available varies with frequency range and a power spectrum for wind is shown usually in frequency or wave number as in Fig. 1(b). At low frequencies the energy content present in eddies represents the buoyancy production sub-range due to changes in density as well as heat flux. In this region, the spectral curves have logarithmic slope of k^4 that correspond to instabilities caused due to turbulent mass transport. For high values i.e. k^{-1} to k^{-3}, in power spectrum, the turbulent kinetic energy becomes lower in amplitude and represents the viscous dissipation of energy at a specified rate in inertial sub-range. The mid-band values, k^0, depict predominant energy containing range for which the logarithmic slope of curve can appear either as flat top or as a tonal peak.

The power spectra thus obtained varies with wave number, k and its power. It must be noted that decay of coherent turbulent structure is found maximum between k^{-4} *to* k^{-7} in dissipation range while highest energy containing eddies are observed between k^4 *to* k^0 in energy containing range. In Fig. 1(c) the turbulent wind field is illustrated by means of length scale and turbulent eddies in atmospheric boundary layer. The size of eddies vary from large scale, L_0 in which predominant energy resides to micro scale, l_0 in which small energy content is available. Within surface layer the energy transfer rate for turbulent flows at high Reynolds numbers occur from large scale to small scale motions in a successive manner and known as energy cascade. It is thus important to note that Kolmogorov's law is based on energy cascade or dissipation principle in which energy transfer rate occurs due to molecular diffusion within fluid that result in turbulent eddies and independent of kinematic viscosity (Qingshan *et al.*, 2012). Table 1 shows the standard values for surface roughness, z_0 for different terrain conditions according to Davenport (1961) and ESDU (1978). The uncertainties in Davenport roughness classification are based on power law model to determine the vertical wind shear or velocity profile.

The exponents in power law vary according to reference surface roughness, z_0 from Counihan (1975) by Eq. (1) and power law by Eq. (2.11) in Bossanyi *et al.* (2001),

$$\psi = 0.24 + 0.096 \cdot \log10(z_0) + 0.016 \cdot \log10(z_0)^2 \qquad (1)$$

where ψ is the power law exponent, z_0 is surface roughness in m. This surface roughness is based on wind speed profile measurement and derived by applying Fast Fourier Transform (FFT) transform on long term measured wind data in order to filter de-trended data from measured time series.

3. Methods

Turbulence prediction using theoretical methods relies on statistically stationary processes while experimental methods needed to improve accuracy are possible using hot wire anemometry (HWA), particle image velocimetry (PIV), laser measurement techniques (LIDAR). Turbulence models based on mixing length region was first proposed by Prandtl (1925) which suggest that turbulent or eddy viscosity is anisotropic in nature. This region is special and analogous to molecular diffusion in kinetic theory of gases and expresses velocity gradients to smaller scales in the boundary layer. Therefore, simulating different length scales of order O(10 m) to O(10^6 m) based on URANS or DNS, and LES methods requires very high computational cost (Ferziger and Peric, 2002; Xu *et al.*, 2019; Worsnop *et al.*, 2017). Hence use of empirical methods to predict turbulence characteristics up to 1 km scale within atmospheric boundary layer is preferred. As turbulence prediction relies mainly on the length scale parameter, a power spectral density (PSD) function is critical to analyze the energy content in the form of large or small scale eddies in atmosphere.

Table 1 - Comparison of surface roughness for different types of terrain derived experimentally with standard surface roughness (Wieringa, 1992).

	Standard roughness, m	Experimentally determined surface roughness, m			
Type of terrain	z_0	Davenport (1961)	Oke (1978)	ESDU (1978)	Cook (1985)
Cities, forests	1.1	0.7	1.0-6.0	0.6-0.9	0.8
Suburbs, (Country side)	0.6	0.3	-	0.4-0.6	0.3
Village country side	0.04-0.18	0.1	-	0.4	0.3
Open farmland	0.034	0.05	0.04-0.2	0.05-0.1	0.03
Flat grassland	0.013	0.01	0.04-0.1	0.008	0.012
Flat desert, open sea	0.003	0.001	0.0003	0.0001	0.003

3.1. Von Karman and Kaimal models

In the present section empirical methods proposed by Kaimal, Von-Karman spectra are expressed in both generalized forms for different length scales and surface roughness. These empirical formulations can be derived either from measured data of length scales in a site or obtained from regression equations which are function of wave number and friction velocity with predefined coefficients for numerator and denominator.

$$\frac{nS_u(z,n)}{{u_*}^2} = \frac{an}{n(c+bn^d)^e} \tag{2}$$

$$\frac{nS_u(z,n)}{\sigma_u^2(z)} = \frac{an}{n(c+bn^d)^e} \tag{3}$$

where n is the frequency, $S_u(z, n)$ is the power spectral density (PSD) function of longitudinal velocity component, u. The coefficients, a, b, c, d and e are coefficients for the spectral frequency range which can be obtained using least square regression method or derived from wind tunnel test data (Wieringa, 1992) It can be seen that Eq. (2) is dependent upon the friction velocity for surface boundary layer, while the Eq. (3) is function of standard deviation of longitudinal velocity component. So for given mean wind speed the PSD is expressed in terms of length scale or surface roughness parameters.

3.2. Kolmogorov's law for turbulent energy

Kolmogorov (1991) derived a generalized formula for energy spectra for turbulent kinetic energy in atmosphere. Although this law is not exact in nature it provided an understanding to viscous dissipation of energy per unit volume in form of vortices or eddies that could exist at different time scales. Hence it can be considered that turbulence in atmospheric boundary layer follows the Kolmogorov $-5/3^{rd}$ law which states that spectral energy content is function of turbulence dissipation rate and given by Eq. (4)

$$E\alpha \quad C\varepsilon^{2/3}n^{-5/3} \tag{4}$$

where E is the spectral energy $(m/s)^2$, C – Kolmogorov's constant ~ 1.5 to 1.7 and ε is the viscous dissipation of turbulent kinetic energy or energy transfer rate. (Qingshan *et al.*, 2012; Kolmogorov, 1991) As turbulence properties for fluid are highly stochastic and anisotropic in nature it is often normalized with respect to the variance of longitudinal wind. Therefore, a normalized turbulence power spectrum better represents the characteristics of turbulent energy production or dissipation of energy in atmospheric boundary layer. An isotropic turbulence spectrum has constant variances for three velocity components, ${\sigma_u}^2$, ${\sigma_v}^2$ and ${\sigma_u}^2$ but for measured time series data the variances are seldom constant indicating anisotropic nature of turbulence. These spectra also obey Kolmogorov law, $k^{(-5/3)}$ for high frequencies or wave numbers with logarithmic slope corresponding to −2/3. Empirical evidence also suggests that for stably stratified shear flows in atmosphere, a critical value of gradient Richardson number, $Ri > Ri_c$ indicates a transition from turbulent to laminar flows, and vice-versa when $Ri < Ri_c$. Hence Richardson number is an important parameter for determination of flow stability in atmosphere.

3.3. Estimation of turbulence intensity

The turbulence intensities for the neutral atmospheric surface boundary layer can be computed from Eq. (5) to Eq. (7). Here $n = fL/U$ and represents the dimensionless frequency.

$$I_u = \frac{\sigma_u}{\overline{U}} \tag{5}$$

$$I_v = I_u\left[1 - 0.22\cos^4\left(\frac{\pi z}{2h}\right)\right] \tag{6}$$

$$I_w = I_u\left[1 - 0.45\cos^4\left(\frac{\pi z}{2h}\right)\right] \tag{7}$$

$$\sigma_u = \frac{7.5\eta\left[0.538 + 0.09\ln\left(\frac{z}{z_0}\right)\right]^p u_*}{\left[1 + 0.156\ln\left(\frac{u_*}{f_c z_0}\right)\right]} \tag{8}$$

$$\eta = 1 - \frac{6f_c z}{u_*} \tag{9}$$

$$p = \eta^{16} \tag{10}$$

Equation (5) to Eq. (7) represents the turbulence intensities in longitudinal, lateral and vertical directions for a point above ground in surface layer according to IEC (1999) standard. Eq. (8) to Eq. (10) evaluates the standard deviation of longitudinal component of wind and expressed in terms of Coriolis parameter, f_c. The variables z, z_0 are surface roughness parameters, h is the height of boundary layer and u_* is the friction velocity, in m/s defined in terms of Von Karman constant (Bossanyi *et al.*, 2001). L_{1u} and L_{2u} are the Euro and ESDU (1985) integral length scales in longitudinal direction defined for Kaimal and Von Karman spectrum.

3.4. Summary of empirical methods studied

In this section we list the empirical spectra for analyzing the turbulent wind field, based on the Kaimal and isotropic Von Karman spectra. The spectra are expressed in terms of integral length scales, standard deviation of longitudinal velocity component and non-dimensional frequency.

$$\frac{nS_u(n)}{\sigma_u^2} = \frac{4f\frac{L_{1u}}{U}}{\left(1+6f\frac{L_{1u}}{U}\right)^{5/3}} \tag{11}$$

$$\frac{nS_u(n)}{\sigma_u^2} = \frac{4f\frac{L_{2u}}{U}}{\left(1+70.8\left(f\frac{L_{2u}}{U}\right)^2\right)^{5/6}} \tag{12}$$

$$\frac{nS_u(n)}{\sigma_u^2} = \frac{4f\frac{L_{2u}}{U}}{\left(1+50.8\left(\frac{fL_{2u}}{U}\right)^2\right)^{5/6}} \times \phi \times \frac{\left[0.75+15\left(\frac{fL_{1u}}{U}\right)^2\right]}{\left[(1+70.8\left(\frac{fL_{2u}}{U}\right)^2\right]} \tag{13}$$

$$\frac{nS_u(n)}{\sigma_u^2} = \frac{200f}{(1+50f)^{5/3}} \tag{14.1}$$

$$f = \frac{nZ}{U(Z)} \tag{14.2}$$

$$\frac{nS_u(n)}{\sigma_u^2} = \frac{4x^2}{(2+x^2)^{5/6}} \tag{15.1}$$

$$x = \frac{1800n}{U(10)} \tag{15.2}$$

$$\frac{nS_u(n)}{\sigma_u^2} = \frac{4x^2}{(1+x^2)^{4/3}} \tag{16.1}$$

$$x = \frac{1200n}{U(10)} \tag{16.2}$$

$$\frac{nS_u(n)}{\sigma_u^2} = \frac{6.868f\frac{L_{1u}}{U}}{\left(1+10.302f\frac{L_{1u}}{U}\right)^{5/3}} \tag{17.1}$$

$$f = \frac{0.1456Z}{L(Z)} \tag{17.2}$$

The wind power spectra density (PSD) functions proposed by various authors viz. Kaimal (1972), Von Karman (1948), Jing and Lee (1998), Simiu (1974), Harris (1971), Davenport (1961) and Solari (1987) is based on the integral length scale, dimensionless frequency and surface roughness and given by Eq. (11) to Eq. (17). It can be noted that longitudinal velocity component for each spectra is useful for predicting the natural events like buffeting phenomenon observed due to free turbulence, wind induced vibrations that cause flutter and wake galloping effects observed on slender bridge decks or sky scraper building structures. The wind PSD thus allows the designers or civil architects to understand the natural frequencies of structures at a given mean wind speed for a location.

3.5. Proposed empirical methods based on Von-Karman and Kaimal spectra

Expressions proposed for the power spectra of wind velocity components, <*u*>, <*v*>, <*w*> and the cross spectra, <*u*, *w*> for an experimental site is given by Eq. (18) to Eq. (25):

$$< u > = \frac{115n}{(1+30n)^{5/3}} \tag{18}$$

$$< v > = \frac{17n}{(1+9.5n)^{5/3}} \tag{19}$$

$$< w > = \frac{2.1n}{(1+5.3n)^{5/3}} \tag{20}$$

$$< u, w > = \frac{-14n}{(1+9.6n)^{2.4}} \tag{21}$$

$$< u > = \frac{120n}{(1+50n)^{5/4}} \tag{22}$$

$$< v > = \frac{10n}{(1+10.5n)^{5/4}} \tag{23}$$

$$< w > = \frac{2n}{(1+5.3n)^{5/4}} \tag{24}$$

$$< u, w > = \frac{-6n}{(1+4n)^{2.4}} \tag{25}$$

The wind PSD for velocity components in present study to estimate the turbulent fluxes is given from the Eq. (18) to Eq. (20) and indicates the longitudinal, lateral and vertical velocity components of Kaimal category. Eq. (21) shows the cross spectra of longitudinal and vertical velocity components. Similarly, it can be seen that Eq. (22) to Eq. (24) denotes the longitudinal, lateral and vertical velocity components and belongs to Von-Karman category. On the other hand cross spectra of vertical and longitudinal components are shown by Eq. (25). Although the general forms of the proposed spectra closely resemble with Von Karman and Kaimal categories, the coefficients in spectra are different and assumed to be that of model spectra by Simiu and have same functional form.

$$C_u(r,n) = \exp\left[-8.8g\Delta r\sqrt{\left(\frac{0.12}{L_u}\right)^2 + \left(\frac{n}{\overline{U}}\right)^2}\right] \quad (26)$$

$$C_u(j,k) = exp\left[-C\frac{nd_{jk}}{U}\right] \quad (27)$$

$$C = 12\left(\frac{d_{jk}}{z}\right)^{0.25} \quad (28)$$

The coherence function is an exponential decaying according to IEC (1999) standard and given by Eq. (26). The coefficient, $-8.8.\Delta r$ represents coherence decay and Δr is function of horizontal separation distance orthogonal to wind. L_u is the local length scale evaluated using the Eq. (2.36) in (Bossanyi *et al.*, 2001) and n is the frequency. However according to the Kaimal (1972) turbulence model, the coherence function is given by the Eq. (27) and decay parameter from Solari is given by Eq. (28). Where d_{jk} is the horizontal (lateral) separation distance between two points, j, k in space, z is the surface roughness height in m, U – free stream velocity in m/s.

4. Results and Discussion

Figure 2(a) illustrates the time series of turbulent wind at mean wind speed of 12 m/s was simulated for 60 s using Von Karman (1948) and Kaimal (1972) models in MATLAB 2019 software. It can be seen that both spectra have been evaluated at high or severe turbulence intensities viz. severe turbulence level (50%) and verified with the simulated results by Shigeo and Metwally, (2018) as shown in Fig. 2(b). Both outputs agreed strongly for the duration, but Von Karman showed better correlation with for entire duration of 60 s. It can be seen that the wind speed varied from as low as 10 m/s and reached a high value of 13 m/s within 20 s.

This shows the gust occurrence has higher probability at severe turbulence intensities. Also Fig. 3(a) and Fig. 3(b) compares time history of longitudinal wind simulated using Von Karman and Kaimal models for a mean wind speed of 12 m/s, at integral length scale of 140 m, and for three different turbulence intensities. Results are compared with time series trend of Shigeo and Metwally, (2018) as shown in Fig. 3(c) which indicates that present simulation outputs are suitable for certain applications like wind turbine load modeling and wind data measured by met mast at different heights. So, auto-correlation of averaged wind speeds measured at different heights for a given terrain is a useful method in estimating the rotor inflow or velocity gradients for a wind turbine operating within the eddy surface layer. Regardless of type of terrain, data measured from weather centers are processed for aggregate errors and use complex numerical weather prediction algorithms to improve the quality of predictions.

According to IEC 61400-1 design standards for wind turbines, Mann (1994) and Kaimal (1972) turbulence spectra are recommended for extreme and fatigue load validation in wind turbine design. Additionally it can be seen from Fig. 2(b) and Fig. 3(c) that results by Shigeo and Metwally (2018) have shown that non-linear nature of turbulence statistics at different turbulence intensities at a given roughness class can be predicted well using Von-Karman and Kaimal models. Cross-correlated and auto-correlation data of wind speed power spectra, as well as coherence function which is a correlation between two points in space for wind fluctuations in 3D wind field is used for fatigue load estimation of wind turbine structures and also includes extreme wind speeds in a gust occurrence. Several computer simulations and wind tunnel test results have proved that Von Karman model better predicts the turbulence statistics in atmosphere for representative integral length scales (Roberto *et al.*, 2016). In the present analysis of longitudinal wind speed time series, a horizontal (lateral) separation distance of 1 m has been used for both Von Karman and Kaimal models. For most wind turbine applications a Kaimal model fits accurately with

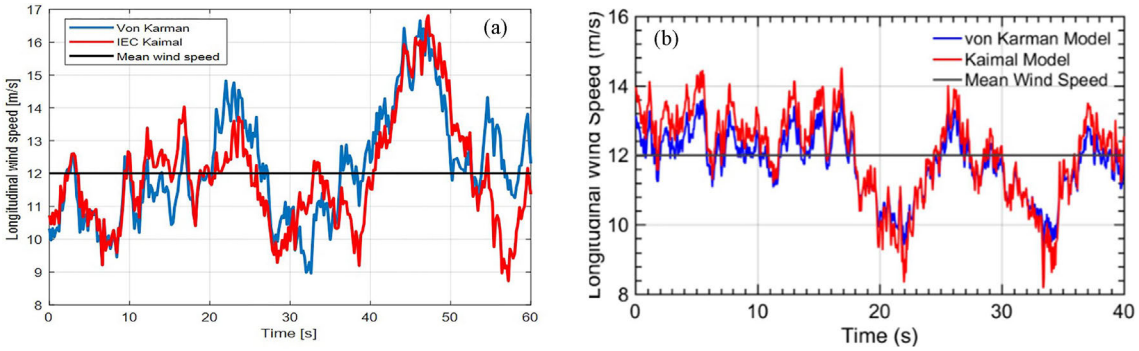

Figure 2 - Comparison of computed time series of Longitudinal wind speed, (U+u) m/s at severe turbulence levels (50%) for a mean wind speed of 12 m/s in MATLAB 2019 software (a) using Von Karmal (1948) and Kaimal (1972) model (b) results of Shigeo and Metwally (2018) using Von Karman and Kaimal model at 50% turbulence intensity.

the practical or measured data of atmospheric turbulence (Bossanyi *et al.*, 2001). From Fig. 2(a) and Fig. 3(a) the fluctuations in wind speed occur randomly and reach a low of 9 m/s and high of 17 m/s and also show gust occurrence. It is useful to know maximum gust wind speed by means of gust factor. This factor is function of turbulence intensity at a given site and expressed as ratio of gust wind speed to hourly mean wind speed. It is important to note that Veers approach for 3D simulation is based on the method by Shinozuka and Jan (1972) which suggests that the fundamental input is wind speed PSD. A point on 3D wind grid is evaluated by correlated spectral matrices, the diagonals of which represent the PSD. Further each diagonal term is cross spectrum of two points i and j defined in terms of PSD and coherence function within grid. As mentioned in section 3.5 the coherence function is frequency dependent measure of correlation of wind speeds at two points in space which varies in exponential manner and given by Eq. (4.1) in (Veers, 1988) However according to Solari (1987) the coherence function is dependent upon both spatial separation distance and coherence decay parameter (Gourdeau *et al.*, 2018). In homogeneous turbulence, coherence function is normalized cross-spectrum of u and w components of wind speed. Several pilot runs of computer simulations were conducted using randomly generated seeds to attain threshold values for a mean wind speed of 12 m/s and the results shown in Fig. 4 are the values of longitudinal, lateral and vertical wind components evaluated at 10% turbulence intensity for 60 s duration. A similar process was implemented to obtain the results shown in the Fig. 2(a), Fig. 3(a) and Fig. 3(b). It can be seen that variances of velocity components follow the trend $\sigma_u^2 > \sigma_v^2 > \sigma_w^2$ and therefore be considered anisotropic in nature. A large variance for u components shows the extent of wind fluctuations from the mean value of wind speed while the variance is smallest for w component. For different turbulence intensities both Von Karman and Kaimal showed high differences in longitudinal component of wind field. This plays critical role in turbines structural response and estimation of fatigue and extreme loads behavior in turbine design (Shigeo and Metwally, 2018) For instance, fatigue study by Shigeo and Metwally (2018) showed that a small increase in turbulence intensity level, from 1% to 10%, a significant reduction of time to failure of wind turbine components were observed. Particularly blades of wind turbine are more sensitive to turbu-

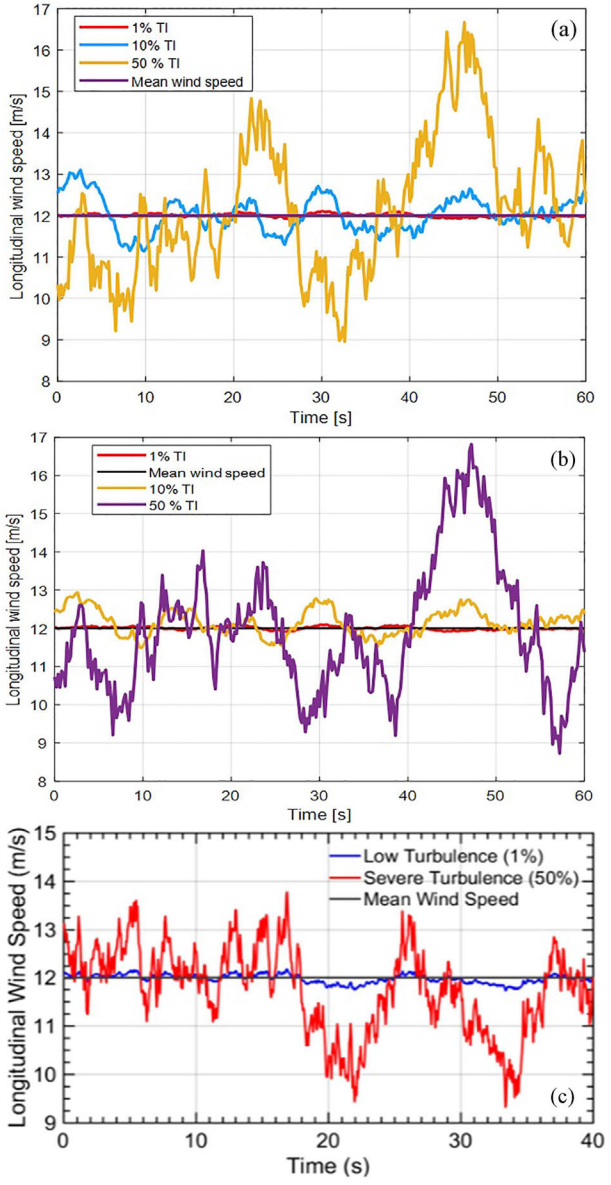

Figure 3 - Comparison of computed time series of Longitudinal wind speed, (U+u) m/s at three different turbulence intensities, low (1%), medium (10%) and severe turbulence levels (50%) for a mean wind speed of 12 m/s (a) using Von Karman (1948) model (b) Kaimal (1972) model (c) results of Shigeo and Metwally (2018) using Von Karman (1948) model at 1% and 50% turbulence intensities.

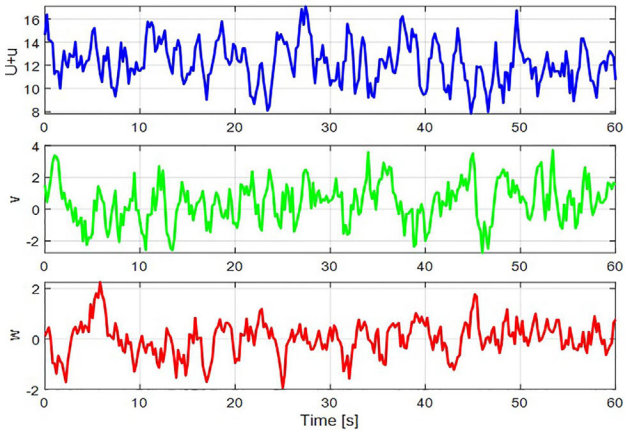

Figure 4 - One-minute time history of longitudinal wind speed, (U+u), lateral and vertical velocity components at 10% turbulence intensity, for mean wind speed of 12 m/s simulated in MATLAB 2019 using Eq. (15) to Eq. (17).

lence and subjected to higher fluctuating loads (Bhargava *et al.,* 2020; Nukala and Maddula, 2020; Bhargava *et al.*, 2019; Bhargava and Samala, 2019). Further, the damage equivalent loads (DEL) predicted by Von Karman and Kaimal turbulence spectra in the study were found to agree within 5% of peak values for different turbulence intensities. In Fig. 2(a), Fig. 3(a) as well as in Fig. 4, a linear down trending can be observed after 20 s. Further from Fig. 4 it can be noted that lateral and vertical wind components, *v* and *w* seem to vary with a phase change of 180° for the first 5 s of simulation. After 5 s linear down trending is observed for vertical component, *w* and after 20 s to 25 s for the longitudinal component, U+u. cosine type oscillations are observed with random phase angles at different time intervals for *u* and *v* components in simulation. The amplitudes of oscillations for the wind speed components are specified according to the coefficients of empirical PSD functions and given by Eq. (15) to Eq. (17) given in section 3.4. The cross correlated wind spectra, <*u, w*> is given by Eq. (18).

The gust behavior can be modeled based on the gust factor that varies with length scale. A gust factor is a ratio of gust wind speed to mean wind speed. Typically a 3 s gust averaging period is suitable for extreme load analysis and taken as standard for civil engineering structures like buildings. Sometimes a 10 s standard is also used for highly damped structure such as tower or for entire rotor of a wind turbine in the event of long gust durations. This indicates wind gusts of different sizes in space represents the time averaging of gust duration and its impact on structural loads is critical in wind turbine design. From Fig. 5(a) the gust factor is evaluated as function of gust duration from 3% to 12.5% turbulence intensities given by Eq. (2.40) given in (Bossanyi *et al.*, 2001). It can be noted that for higher turbulence intensities, the gust factor increases when the gust durations are short than when it is long. From Fig. 5(b) the gust factor is plotted according to Eq. (19) given in (Frandsen *et al*., 2008). It is expressed in terms of integral length scale of turbulence and mean wind speed measured at meteorological mast. The gust factor is demonstrated at different wind speeds for a rotor cut-off frequency of 0.05 Hz that corresponds to pre-averaging period of 10 s gust duration assumed for a wind turbine rotor with a diameter of 50 m. Also from Fig. 5(b) the slope of gust factor is found to remain constant beyond 60 m height above ground for different mean wind speeds suggesting that gust factor influence on the variance of wind speed fluctuations with height is negligible.

More accurate turbulence information is possible via velocity spectra of components, *u, v, w* and its correlations. Fig. 6(a) shows the auto and cross spectra of type I for longitudinal, lateral and vertical velocity components given by Eq. (18) to Eq. (21) while Fig. 6(b) shows type II auto and cross spectra of wind components obtained using Eq. (22) to Eq. (25). It can be noted that both the types can be regarded as Von Karman type spectra, where *n* is *fz/U*. Further, from Fig. 6(a) and Fig. 6(b) both spectra types have been fitted with experiment dataset obtained for *u, v* and *w* components. It can be seen from Fig. 6(a) that for the spectra represented by Eq. (18) to Eq. (21), the turbulent kinetic energy in longitudinal velocity component is higher in production sub-range while for lateral and vertical velocity components are less scattered in that frequency range. This phenomenon is not seen in viscous dissipation range. Similarly from Fig. 6(b) it can be noted the wind power spectra represented by Eq. (21) to Eq. (24) agreed within 1% of measured data through the whole of the production range, inertial sub range and viscous dissipation range respectively. This shows that turbulence production in the surface layer is predicted well for the heights that are important for structures such as wind turbines and most industrial dwellings.

Further from Fig. 6(a) it can be seen that measured data scatter for longitudinal wind component with respect to the calculated spectral peak differ by more than 50% in production and inertial sub-range. This difference found in

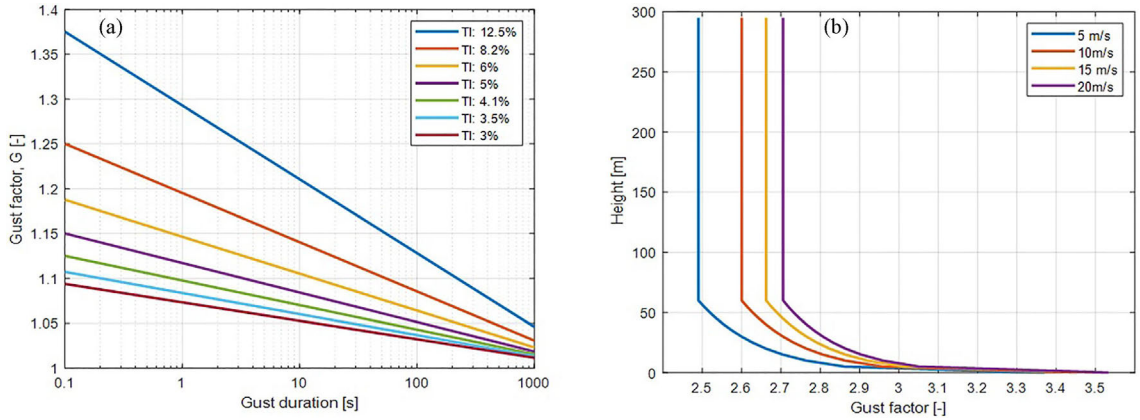

Figure 5 - (a) Gust factor at different turbulence intensities and gust duration (b) Gust factor as function of height for wind speeds of 5 m/s, 10 m/s 15 m/s and 20 m/s.

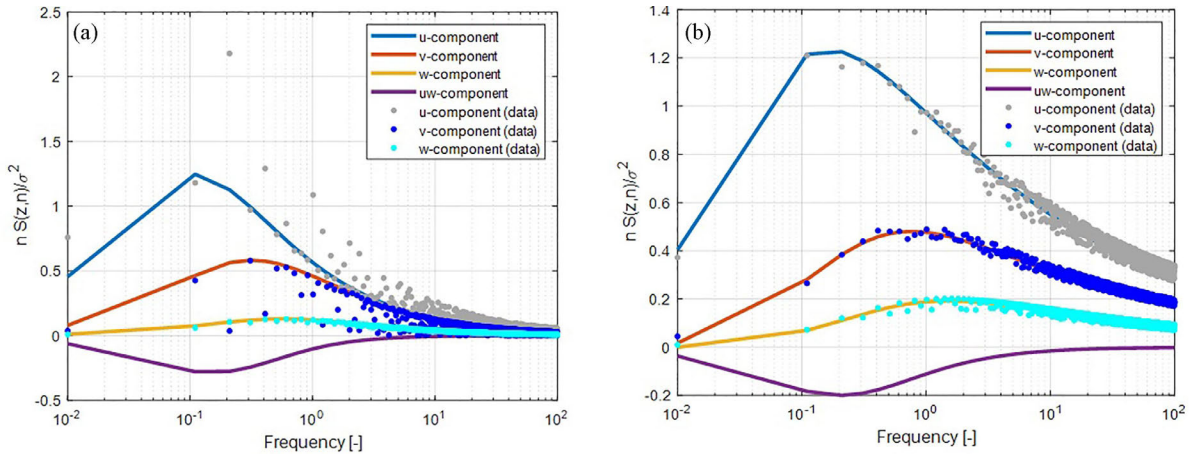

Figure 6 - Normalized velocity component spectra, *u, v, w* and cross spectra, *u*-*w,* functions, for z = 10 m and U = 20 m/s given by (a) Eq. (18) to Eq. (21) (b) Eq. (22) to Eq. (25).

high frequency or viscous dissipation range is less than 5%. However, for lateral and vertical wind components, the difference between the measured data and calculated spectral peak is about 5%. From Fig. 6(b) it can be seen that the difference in measured data and calculated spectral peak differed by approximately 10% for all three wind speed components. Primarily the reason for this deviation could be attributed to the averaging time periods used for the measured data. Secondly, it can be said that there could uncertainties in the coefficients obtained during the regression method in calculated power spectra which lead to over prediction of power spectra results in high frequency or viscous dissipation region.

Also from Fig. 6(a) all three velocity component spectra decay at high frequencies, implying turbulence dissipation in inertial sub-range and dissipation range, however for spectra in Fig. 6(b) the dissipation of turbulent kinetic energy occurs at lower scale. This is evident for complex coastal terrains where the large scale turbulent eddies are found to propagate over large distances before they attain equilibrium with land surface while small eddies get adjusted rapidly at a low fetch according to Monin-Obhukov (M-O) similarity law. So, a Von Karman model is more suited for describing the turbulence statistics for convective boundary layer. Turbulence anisotropy in boundary layer for such environments are useful for load modeling of offshore wind turbines but for altitudes less than 150 m, Kaimal model is better suited for determining local similarity in coherent turbulence structures and hence preferred for fatigue load prediction of land based wind turbines.

Fig. 7(a) shows the comparison of normalized auto spectra using custom turbulence model with Von Karman and Kaimal models using IEC (1999), Euro and Danish (DS472) integral length scales (Bossanyi *et al.*, 2001) The custom model proposed by Jing and Lee (1998) is defined by Eq. (13) in section 3.4 in which ϕ is the random noise to produce turbulence over whole frequency region. It must be noted that frequency is normalized with respect to length scale and given by $n = fL/U$. To generate random noise, MATLAB function, *rand* was run for different seeds at different intervals for a given wind speed. From the Fig. 7(b) a comparison of Harris, Davenport and Simiu turbulence spectra with Kolmogorov micro-scale $k^{-5/3}$ for the inertial and dissipation sub-range is shown. It can be seen that logarithmic slope of Harris and Simiu spectra coincides well with Kolmogorov $k^{-5/3}$ law at low frequencies compared to remaining two spectra. For high frequencies however, slight deviations were observed between Simiu (1974) and Davenport (1961) spectra. Similarly from Fig. 7(a) for low frequencies Von Karman (1948) model also showed deviation with Kaimal (1972) model and underestimates the buoyancy contribution to turbulence. In a Kolmogorov sense, it is similar to suppression of the turbulent energy production that is apparent during night times within atmospheric boundary layer. A similar trend can also be seen using custom model proposed by Jing and Lee (1998). However, in the mid and low frequency region, both Von Karman and custom models overestimates the turbulent kinetic energy of along wind component compared to Kaimal model. Also from Fig. 7 (a) appropriate length scales recommended by ESDU (1985) and IEC (1999) for Von Karman model given by Eq. (2.28) in (Bossanyi *et al.*, 2001) were used to determine the u-component spectra and to compare the logarithmic slope of the curve in buoyant turbulent region. Additionally, Euro and Danish (DS472) length scales have also been used to compare custom spectra proposed by Jing and Lee (1998) and given by Eq. (13) in section 3.4 with both Von Karman and Kaimal models. This is done to check how length scales affect the turbulent kinetic energy production and its viscous dissipation at high frequencies in boundary layer.

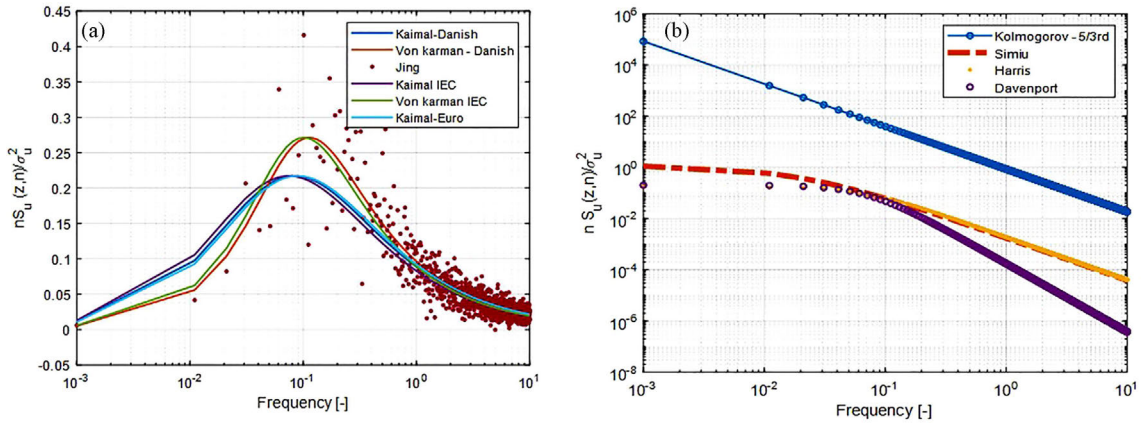

Figure 7 - (a) Normalized empirical turbulence spectra for different integral length scales at a z_0 value of 0.05 m, at U = 50 m/s (b) Comparison of Davenport (1961) wind codes adopted by China and Canada, Harris (1971), Simiu (1974) wind codes by ESDU (1985) with Kolmogorov's 5/3rd law at U = 50 m/s.

In the energy containing range, the Von Karman spectra predicts large shear generated turbulence than others which implies that energy containing eddies result in peak at specific frequency. This reveals that turbulent eddies are less damped before dissipating into small scale coherent turbulence and therefore provides information for modeling extreme load on structures like slender bridge decks. For integral scales, $L > 600$ m the slope varies as k^{-3} suggested by Shur *et al.* (1966), Lumley (1964) which shows that turbulence decays rapidly showing a turbulent dissipation or faster energy transfer rates in thermally stable or neutrally atmosphere stratification common for wind turbines. Fig. 8(a) shows longitudinal Kaimal spectra for different roughness heights compared to Kaimal (1972) spectra. Fig. 8(b) shows that coherence function is an exponential decaying according to IEC (1999) standard. For higher values of roughness heights, the IEC Kaimal coherence function approaches zero for frequencies greater than 0.05 Hz. This also suggests that spatial structure of turbulence in surface layer in atmosphere become highly random and result in wind field fluctuations in the presence of wakes or obstacles.

Fig. 9(a) shows the plot of normalized coherence decay function as function of separation distance, Δr, at low frequency, 0.01 Hz and based on either Kaimal or Von Karman spectra according to IEC (1999). The Fig. 9(b) illustrates coherence decay function as function of horizontal separation distance, d_{jk} at frequency, 0.01 Hz using Solari (1987) model. For IEC (1999) standard coherence function, it can be seen that as surface roughness heights increase, the coherence decay is reduced as much as 100% at small horizontal separation distance, $\Delta y < 10$ m, while for large horizontal separation distances, $\Delta y > 10$ m, the decay approaches to zero at increased roughness heights. However, this trend is not observed for Solari (1987) decay function for which there is negligible change of coherence, less than 10% for varying roughness heights. This suggests that Solari model underestimates the turbulence structure used in predicting the anisotropic nature of turbulence.

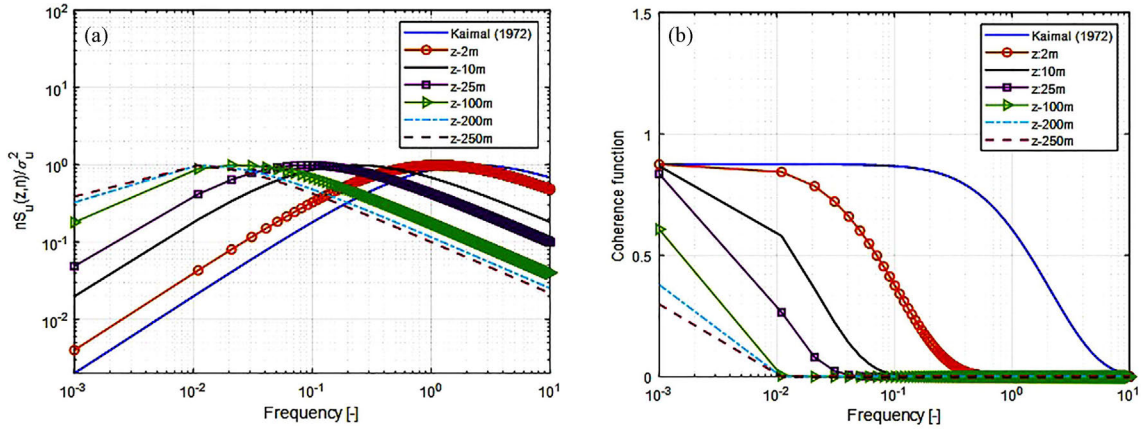

Figure 8 - Normalized (a) longitudinal IEC Kaimal wind spectra at different roughness heights at U = 50 m/s (b) IEC Kaimal standard coherence function along longitudinal direction, at U = 50 m/s, standard roughness $z_0 = 0.05$ m, separation distance, horizontal $\Delta y = 1$ m, vertical $\Delta z = 1$ m.

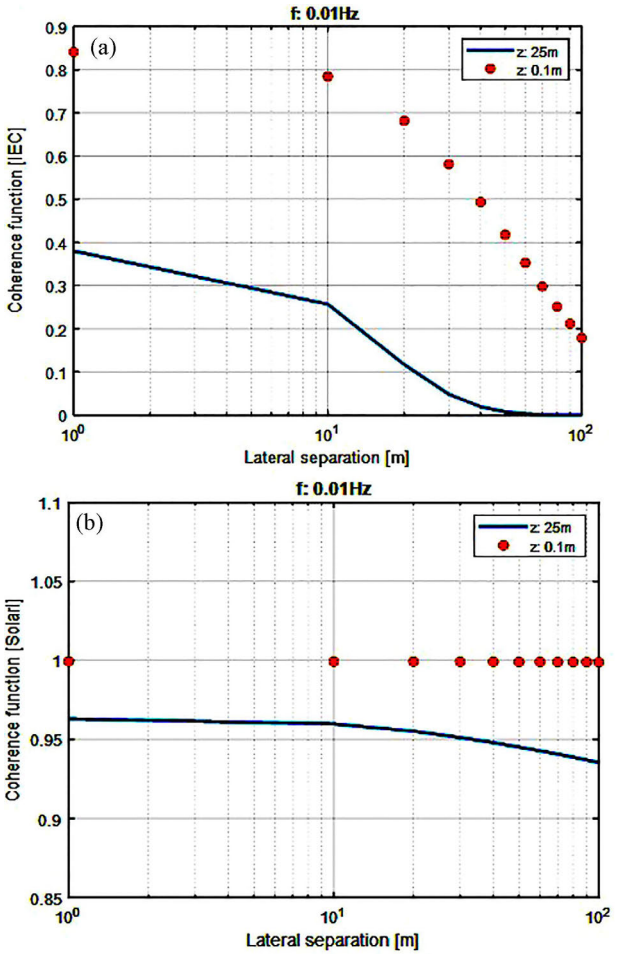

Figure 9 - Comparison of (a) IEC (1999) coherence function at z = 0.1 m and 25 m for 0.01 Hz using Kaimal (1972) spectrum (b) Coherence function at z = 0.1 m , 25 m for 0.01 Hz using Solari (1987) decay parameter at gust wind speed of 70 m/s.

Fig. 10(a) and Fig. 10(b) show the ESDU (1985) recommended longitudinal, lateral and vertical turbulence intensities as well as integral length scales at different heights above ground for reference surface roughness length of 0.05 m given in Table 1 in section 2. From Fig. 10(a) it can be seen that with increase in heights up to 50 m, the values for I_u and I_w turbulence intensity reach 12% and 16% while the lateral turbulence intensity values increase dramatically up to 20%. For heights beyond 50 m, the slope of I_w is found to remain constant while I_u is found to reduce down to value of 10%. Similarly from Fig. 10(b) the length scales in longitudinal and lateral directions are found to increase exponentially while it increases linearly for vertical direction. This suggests that both turbulence intensity and length scales affect the turbulence characteristic in atmospheric boundary layer. Fig. 10 (c) shows the elevation map for the Jaisalmer district located in state of Rajasthan. It has mean elevation of 223 m with met masts height up to 90 m are installed for

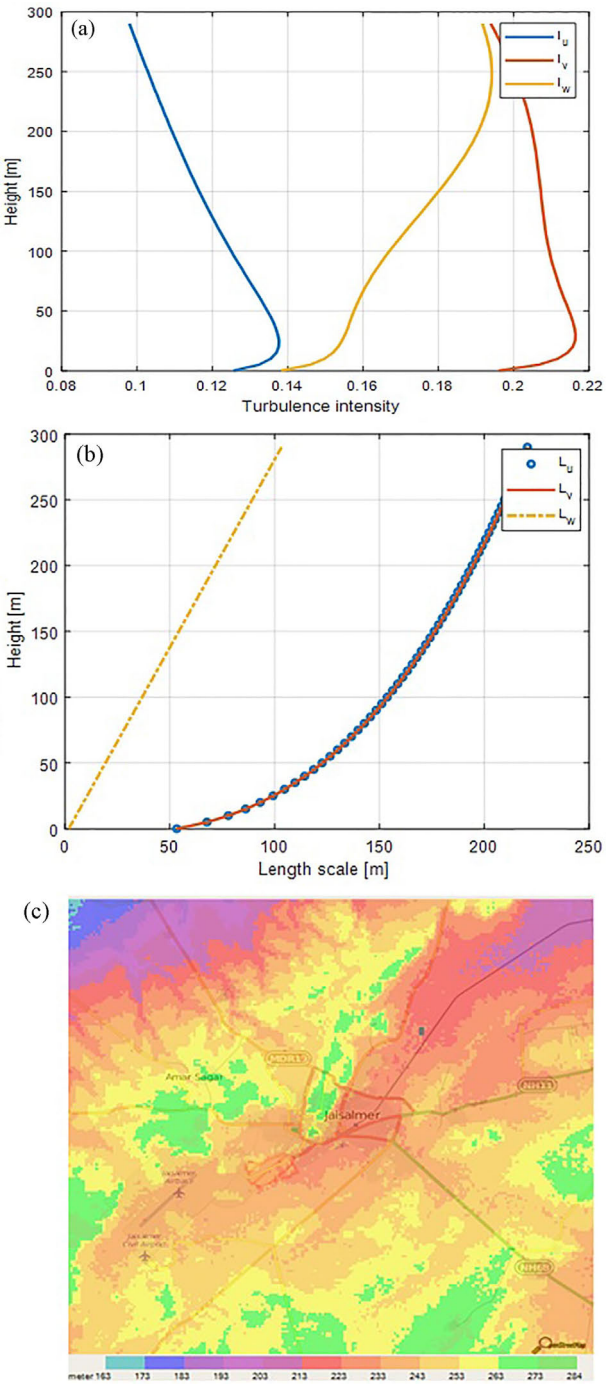

Figure 10 - Illustration of (a) longitudinal (I_u), lateral (I_v) and vertical (I_w) turbulence intensities according to ESDU (1985), standard for z_0 value of 0.05 m (b) ESDU (1985) length scales for z_0 value of 0.05 m respectively at 26.91° north latitude (c) Elevation map of Jaisalmer site in Rajasthan with a mean elevation of 223 m (Source: www.floodmap.net).

measurements. The geographical coordinates are 26.91° N, 70.9° E.

Fig. 11(a) and Fig. 11(b) show contour plot of normalized wind speed spectra according to IEC Kaimal for

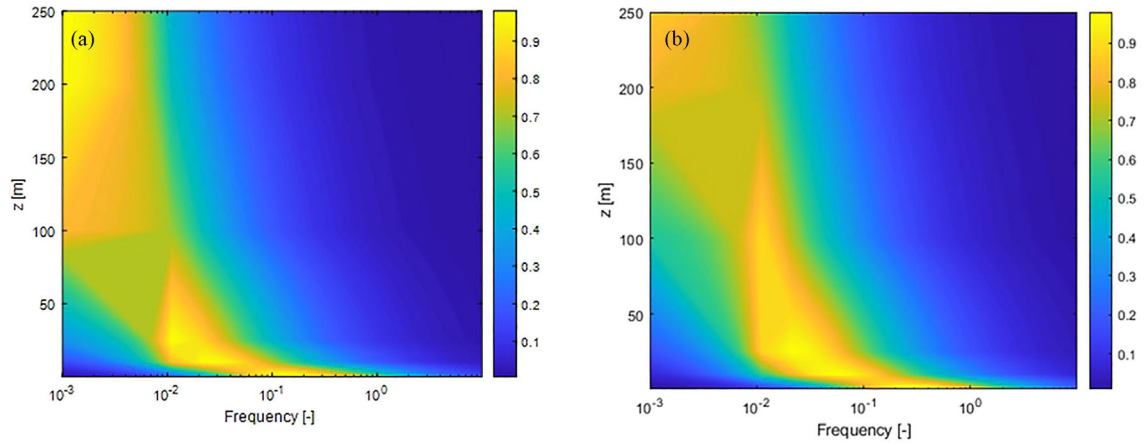

Figure 11 - Contour plot of normalized longitudinal wind spectra using IEC Kaimal method at different roughness heights (a) for free stream velocity of 10 m/s (b) for free stream velocity of 15 m/s at separation distance, $\Delta y = 1$ m, $\Delta z = 1$ m, standard roughness, $z_0 = 0.05$ m.

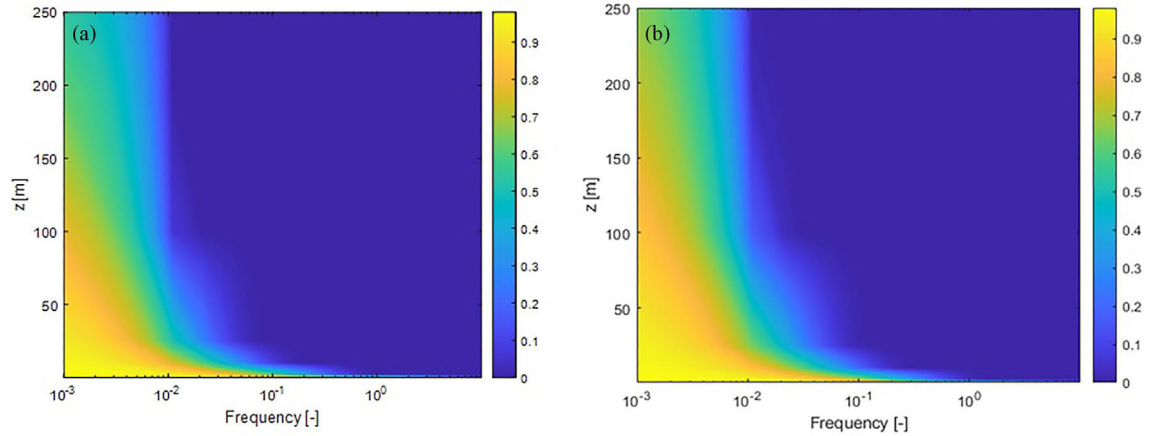

Figure 12 - Contour plot of normalized coherence function for longitudinal wind using IEC Kaimal method at different roughness heights above ground (a) for free stream velocity of 10 m/s (b) for free stream velocity of 15 m/s at lateral separation distance, $\Delta y = 1$ m, $\Delta z = 1$ m, standard roughness, $z_0 = 0.05$ m.

$z_0 = 0.05$ m. It is evident that with increase in height above ground, IEC Kaimal predicts the production of turbulent kinetic energy in buoyant region is higher and extends to mid frequencies of the spectra. This shows that turbulent eddies in buoyant sub-layer region vary with length scales. Further from Fig. 12(a) and Fig. 12(b) it can be noticed that with increase in height above ground, the trend for spatial coherence between two points is high at low frequencies. Thus, turbulence anisotropy and spatial coherence of turbulence structure in atmospheric boundary layer predominantly vary with length scale and surface roughness.

5. Conclusions & Future Work

- An empirical study of atmospheric turbulence within surface boundary layer was conducted using spectral methods by Kaimal and Von Karman models for roughness heights up to 150 m. Within the surface boundary layer the slope of the Harris and Simiu turbulence spectra in the dissipation range obey Kolmogorov law well than Davenport spectra which suggests that viscous dissipation of turbulent kinetic energy is predicted well in case of Harris and Simiu model.
- The turbulence characteristics for wind speed components for a mean value of 12 m/s at 1%, 10% and 50% (severe) turbulence intensities showed that spatial variance for longitudinal wind speed component differed significantly from lateral and vertical components. For low values of turbulence intensity the wind speed fluctuations from Von Karman and Kaimal predictions were of anisotropic nature. For severe turbulence intensity Von Karman and Kaimal turbulence spectra showed strong agreement with each other.
- The longitudinal coherence function for IEC Kaimal model indicates that for increasing horizontal separation distances and surface roughness, the coherence

decay between two points in spatial grid is found to reduce for IEC coherence decay function but it changed negligibly for Solari model decay function.

- Power spectra density (PSD) for given wind speed showed that most of the turbulent kinetic energy in surface boundary layer is dissipated in form of viscous effects. The effects have predominantly varied according to the length scale and surface roughness parameters. As the part of future work, a comparison of wind power spectra obtained from empirical methods with two parameter Weibull distribution would be useful. This helps to analyze dynamic responses of wind and load spectra on wind turbine structures to greater detail and determine the right type of spectra for given wind speed and terrain type.

Acknowledgements

Authors would like to thank all those who gave valuable feedback for improving the quality of the work.

References

BHARGAVA, V.; KASUBA, S.; MADDULA, S.P.; JAGADISH, D.; KHAN, MD.A. *et al*. A case study of wind turbine loads and performance using steady state analysis of BEM, **International Journal of Sustainable Energy**, v. 40, n. 1, p. 1-20, 2020.

BHARGAVA, V.; SAMALA, R. Acoustic emissions from wind turbine blades, **Journal of Aerospace Technology and Management**, v. 11, n. 1, p. 1-14, 2019.

BHARGAVA, V.; SAMALA, R.; ANUMULA, C. Prediction of broadband noise from symmetric and cambered airfoils, **INCAS Bulletin**, v. 11, n. 1, p. 39-51, 2019.

BOSSANYI, E.; SHARPE, D.; JENKINS, N.; BURTON, T. **Wind Energy Handbook**. Chichester: John Wiley & Sons Limited, 2001 .

CHAUDHARY, V.; ABHILASH, A. Literature review: Mitigation of atmospheric turbulence on long distance imaging system with various methods. **International Journal of Science and Research**, v. 3, n. 12, p. 2227-2231, 2012.

CHOUGULE, A.; MANN, J.; SEGALINI, A.; DELLWIK, E. Spectral tensor parameters for wind turbine load modeling from forested and agricultural landscapes, **Wind Energy**, v. 18, n. 3, p. 469-481, 2015.

CHOUGULE, A.; MANN, J.; KELLY, M.; LARSEN, G.C. Simplification and validation of a spectral tensor model for turbulence including atmospheric stability, **Journal of Boundary Layer Meteorology**, v. 167, n. 3, p. 371-397, 2018.

COUNIHAN, J. Adiabatic boundary layer: A review and analysis of data from the period 1880-1972. **Journal of Atmospheric Environment**, v. 9, n. 10, p. 871-905, 1975.

CLEMENT, R.J.; MONCRIEFF, B.J. A functional approach to vertical turbulent transport of scalars in the atmospheric surface layer, **Boundary Layer Meteorology**, v. 173, n. 3, p. 373-408, 2019.

DAVENPORT, A.G. The spectrum of horizontal gushiness near the ground in high winds. **Journal of Royal Meteorological Society**, v. 87, n. 372, p. 194-211, 1961.

DYRBYE, C.; HANSEN, S.O. **Wind Loads on Structures**. Chichester: John Wiley & Sons, 1997.

FERZIGER, J.H.; PERIC, M. **Computational Methods for Fluid Dynamics**, 3rd ed. Berlin: Springer Verlag, 2002.

FRANDSEN, S.; JORGENSEN, H.E; SORENSEN, J.D. Relevant criteria for testing the quality of turbulence models. **Journal of Solar Energy Engineering**, v. 130, n. 3, p. 1-7, 2008.

FRANK, M.W. **Fluid Mechanics**, 7th ed. New York: McGraw Hill, 2011.

GOURDEAU, L.; TCHILIBOU, M.; MORROW, R.; SERAZZIN, G.; DJATH, B. *et al*. Spectral signatures of tropical pacific dynamics from model and altimetry. A focus on meso and sub-meso scale range. **Journal of Ocean Science,** v. 14, n. 5, p. 1283-1301, 2018.

HARRIS, R.I. The nature of wind, The modern design of wind sensitive structures. **Proceedings of CIRIA Seminar**, England, p. 29-55, 1971.

JING, J.J.; LEE, L.Y. A study of along wind speed power spectrum for Taiwan area. **Journal of Marine Science and Technology**, v. 6, n. 1, p. 71-77, 1998.

KAIMAL, J.C.; WYNGAARD, J.C.; IZUMI, Y.; COTE, O.R. Spectral characteristics of surface layer turbulence, **Q.J.R. Meteorological, Society**, v. 98, n. 417, p. 563-589, 1972.

KAIMAL, J.; FINNIGAN, J.J. **Atmospheric Boundary Layer Flows, Their structure and Measurement**. New York: Oxford University Press, 1994.

KOLMOGOROV, A.N. The local structure of turbulence in incompressible viscous fluid for very large Reynolds numbers. **Proceedings of the Royal Society A, Mathematical, Physical and Engineering Sciences**, v. 434, n. 1, p. 9-13, 1991.

LIEN, C.R.; SANFORD, T.B. Turbulence spectra and local similarity scaling in a strongly stratified oceanic bottom boundary layer. **Journal of Continental Shelf Research**, v. 24, n. 3, p. 375-392, 2004.

LUMLEY, J.L. The spectrum of nearly inertial turbulence in a stably stratified fluid, **Journal of Atmospheric Sciences**, v. 21, n. 1, p. 99-102, 1964.

LUNGU, D.; VAN GELDER, P. Characteristics of wind turbulence with applications to wind codes. **Proceedings of the 2nd European and African Conference on Wind Engineering**, Genova, p. 1271-1277, 1997.

MANN, J. The spatial structure of neutral atmospheric surface-layer turbulence. **Journal of Fluid Mechanics**, v. 273, n. 5, p. 141-168, 1994.

MAHRT, L.; SUN, J.; STAUFFER, D. Dependence of turbulent velocities on wind speed and stratification. **Boundary Layer Meteorology**, v. 155, n. 1, p. 55-71, 2015.

MIKKELSEN, T.; LARSEN, S.E.; JORGENSEN, H.E.; ASTRUP, P.; LARSEN, X.G. Scaling of turbulence spectra measured in strong shear flow near the earth's surface. **Royal Swedish Academy of Sciences**, v. 92, n. 12, p. 1-27, 2017.

NUKALA, V.B.; MADDULA, S.P. Influence of rotor solidity on trailing edge noise from wind turbine blades. **Advances in Aerodynamics**, v. 2, n. 1, p. 1-20, 2020.

OLESEN, H.R.; LARSEN, S.E.; HOJSTRUP, J. Modelling velocity spectra in the lower part of planetary boundary layer. **Journal of Boundary Layer Meteorology**, v. 29, n. 3, p. 285-312, 1984.

PANOFSKY, A.; DUTTON, J.A. **Atmospheric Turbulence: Models and Methods for Engineering Applications**. New York: Wiley-Blackwell, 1984.

QINGSHAN, Y.; YUJI, T.; LI, B.; CHEN, B. Statistical spectrum of wind velocity at Beijing meteorological tower. **The 7th International Colloquium on Bluff Body Aerodynamics and Applications**, v. 54, Article 2869, Shanghai, China. 2012.

ROBERTO, W.A.; ALVAREZ, M.G.; DEMARCO, G.; MARTINS, G.N.L.; PUHALES, S.F. *et al.* Employing wind tunnel data to evaluate a turbulent spectral model. **American Journal of Environmental Engineering**, v. 6, n. 4A, p. 156-159, 2016.

SERAFIN, S.; ADLER, B.; CUXART, J.; DE WEKKER, S.F.J.; GOHM, A. **et al**. Exchange processes in the atmospheric boundary layer over mountainous terrain. MDPI, **Journal of Atmosphere**, v. 9, n. 3, p. 1-32, 2018.

SHIGEO, Y.; METWALLY, I. Study of turbulence intensity effect on the fatigue lifetime of wind turbines, Evergreen joint. **Journal of Novel Carbon Resource Sciences & Green Asia Strategy**, v. 5, n. 1, p. 25-32, 2018.

SHINOZUKA, M.; JAN, C.M. Digital simulation of random processes and it applications. **Journal of Sound and Vibration**, v. 25, n. 1, p. 111-128, 1972.

SHUR, G.N.; REITER, E.R.; PINUS, N.Z.; VINNICHENKO, N.K. Power spectra of turbulence in free atmosphere. **Tellus**, v. 19, n. 2, p. 206-213, 1966.

SIMIU, E. Wind spectra and dynamic along wind response. **Journal of the Structural Division**, v. 100, n. 9, p. 897-191, 1974.

SOLARI, G. Turbulence modeling for gust loading. **Journal of Structural Engineering**, v. 113, n. 7, p. 1550-1569, 1987.

SOLTYS, R.; TOMKO, M.; KMET, S. Study of local turbulent wind characteristics and wind velocity simulations. **Building Research Journal**, v. 60, n. 1, p. 31-50, 2012.

SUTTON, O.G. **Micrometeorology**. New York: McGraw-Hill, 1953.

TAYLOR, P.A. Airflow above changes in surface heat flux, temperature and roughness. An extension to include the stable case. **Journal of Boundary Layer Meteorology**, v. 1, n. 4, p. 474-497, 1971.

TEUNISSEN, H.W. Structure of mean winds and turbulence in planetary boundary layer over rural terrain. **Journal of Boundary Layer Meteorology**, v. 29, n. 2, p. 285-312, 1980.

VAN DER HOVEN, I. Power spectrum of horizontal wind speed in the frequency range from 0.0007 to 900 cycles per hour. **Journal of Meteorology**, v. 14, n. 2, p. 160-164, 1957.

VEERS, P.S. **Three Dimensional Wind Simulation**. Sandia Report, SAND88-0152, UC-261v, 1988.

VON KARMAN, T. Progress in structural theory of turbulence. **Proceedings of the National Academy of Science**,v. 34, n. 11, p. 530-539, 1948.

WIERINGA, J. Updating Davenport roughness classification. **Journal of Wind Engineering and Industrial Aerodynamics**, v. 41, n. 3, p. 357-368, 1992.

WORSNOP, R.P.; BRYAN, G.H.; LUNDQUIST, J.K.; ZHANG, J.A. Using large eddy simulations to define spectral and coherence characteristics of the hurricane boundary layer for wind energy applications. **Journal of Boundary Layer Meteorology**, v. 165, n. 1, p. 55-86, 2017.

XU, C.; HAN, X.; LIU, D.; SHEN, W.; LI, L. *et al*. Monin-Obukhov Similarity theory for modeling of wind turbine wakes under atmospheric stable conditions: Breakdown and modifications. **Journal of Applied Sciences**, v. 9, n. 20, p. 1-24, 2019.

Internet Resources

https://www.floodmap.net/?gi=1269507, **Floodmap Pro Jaisalmer**, India Flood Map: Elevation Map, Sea Level Rise Map.

https://www.esdu.com/cgi-bin/ps.pl?sess=unlicensed_1201021131221jwq&t=doc&p=esdu_85020g, ESDU 1985, **Characteristics of atmospheric turbulence near the ground, Part II, Single point data for strong winds (neutral atmosphere) ESDU 85020**, Engineering Sciences and Data Unit, UK.

https://webstore.iec.ch/preview/info_iec61400-1%7Bed3.0%7Den.pdf, **IEC 1999 Wind turbine generator systems, Part-I, safety requirements, International standard 61400-1**, 2nd ed., International Electro-Technical Commission.